Effects of Nanopillars and Surface Coating on Dynamic Traction Force

Stella Pang (pang@cityu.edu.hk)
City University of Hong Kong https://orcid.org/0000-0002-4330-0877
Yijun Cheng
City University of Hong Kong

Article

Keywords: Cell Traction Force, Nanopillars, Surface Coating, Cell Migration, MC3T3-E1 Cell

Posted Date: July 27th, 2022

DOI: https://doi.org/10.21203/rs.3.rs-1868047/v1

Version of Record: A version of this preprint was published at Microsystems & Nanoengineering on January 5th, 2023. See the published version at https://doi.org/10.1038/s41378-022-00473-0.

Abstract

Extracellular matrix serves as a structural support for cells and provides biophysical and biochemical cues for cell migration. Topography, material, and surface energy can regulate cell migration behaviors. The responses of MC3T3-E1 cells, including migration speed, morphology, and spreading on various platform surfaces were investigated. Polydimethylsiloxane (PDMS) micropost sensing platforms with nanopillars, silicon oxide, and titanium oxide on top of the microposts were fabricated, and dynamic cell traction force during migration was monitored. The relationships between various platform surfaces, migration behaviors, and cell traction force were studied.

Compared with flat PDMS surface, cells on silicon oxide and titanium oxide surfaces showed reduced mobility, less elongation, and larger cell area. On the other hand, cells on nanopillar surface showed more elongation, higher migration speed, and smaller cell area compared to cells on silicon oxide and titanium oxide surfaces. MC3T3-E1 cells on microposts with nanopillars exerted larger traction force than those on microposts without nanopillars, as well as having more extensions of filopodia and long protrusions. Understanding the relationships between platform surface condition, migration behavior, and cell traction force can potentially lead to better control of cell migration in biomaterials capable of promoting tissue repair and regeneration.

1. Introduction

The extracellular matrix (ECM) microenvironment provides biophysical and biochemical cues such as topography, stiffness, functional groups, and surface energy for cells.[1,2] These cues can regulate cell proliferation, apoptosis, migration, differentiation, and spreading.[3] Furthermore, cell migration is an essential physiological and pathological process related to embryo development, wound healing, tumor metastasis, and angiogenesis.[4–6] For example, osteoblasts (MC3T3-E1) cells undergo cell migration to form the calcified bone matrix, which is essential for the precise coordination of bone remodeling.[7] Therefore, it is useful to develop artificial ECM with proper topography and surface coating to control cell migration for potential application of regenerative medicine. These artificial ECMs could be used to replace damaged tissues or organs.[8] They can also be applied to study cell biomechanics, which could influence various pathological processes.[9]

Previous researchers have shown that topography and surface chemistry of biomaterials could influence cell migration.[10–12] Platforms with designed topographical features were developed to guide cell migration.[13–15] Mouse osteoblast cells were guided to migrate along with the gratings of specific width and height.[16] In addition, by introducing asymmetrical topography, cells could migrate with better directionality.[14] On the other hand, surface roughness is an essential factor affecting cell migration behaviors.[17] Nanoscale roughness is found to positively affect cell adhesion, growth, and migration.[18] Compared with flat surface or grating topography, platforms with nanoholes or nanopillars could promote the formation of filopodia and long protrusions, thus increased the migration speed of MC3T3-E1 cells.[19]

In addition, the surface chemistry of biomaterials, such as wettability, is known to influence cell responses. The hydrophilic silicon oxide and titanium oxide are often used as coatings for implanted devices due to their good biocompatibility.[20,21] Surface energy on ECM can control fluid interaction, cell adhesion, and protein adsorption, thus influences tissue formation.[22] It had been reported that surface with a contact angle of ~ 70° provided the best control of cell behaviors.[23] Cell adhesion was the highest for contact angle between 60° and 80°, and decreased for larger contact angle. In this work, nanopillars and surface coating were used to change surface energy on platforms, which provided a broader understanding of the interactions between cells and platforms with various surface conditions.

Cells sense the biophysical and biochemical properties of the surface to guide subsequent cellular responses.[24] When cells make contact with a surface, cell traction force is generated by actomyosin interaction and actin polymerization.[25] For example, cells could response to the substrate stiffness through the transmission of cell traction force that affects cell morphology and migration.[26,27] Furthermore, topographical guidance and confinement had been shown to influence the cell traction force.[28,29] Therefore, monitoring cell traction force is critical in understanding cell-ECM interactions.[30]

Nonetheless, most studies of cell traction force using microposts as sensors mainly showed the static traction force of cells on flat polydimethylsiloxane (PDMS) surface without showing traction force distribution overtime on different surfaces.[31] In addition, very little is known about how the dynamic traction force is related to cell migration behaviors on surfaces with different topographies or coatings. In this work, cell migration behaviors were studied systematically on different surfaces, including surfaces with flat PDMS, nanopillars, silicon oxide, and titanium oxide. Subsequently, PDMS micropost sensing arrays with nanopillars and various coatings on top were developed to track the cell traction force of MC3T3-E1 cells. In particular, the relationships between surface conditions, migration behaviors, and traction force were correlated. Cell migration behaviors over time on platforms with different surfaces were analyzed. Cells on microposts with nanopillars were found to exert a larger traction force than on microposts without nanopillars or with oxide coatings. More filopodia and long protrusions were observed on microposts with nanopillars. This comprehensive study of the relationships between surface condition, migration behavior, and cell traction force could help to generate engineered ECM with proper surface conditions that is capable of controlling cell migration to promote tissue repair and regeneration.

2. Experiment And Methods

2.1 Fabrication technology for micropost sensing platforms

Figures 1(a-j) show the schematics of the fabrication technology to pattern nanopillars on top of microposts. Silicon (Si) substrate was cleaned in acetone, isopropanol, and deionized (DI) water for 10 min, and baked at 105 ℃ for 10 min. The hydrophilicity of Si substrate was increased using an O_2 plasma with 20 sccm O_2, 100 mTorr, and 100 W radio frequency (RF) power for 5 min. SU-8 polymer was spin-coated on the Si substrate and baked at 65 and 95 ℃ for 2 min each. SU-8 nanopillars, which were

280 nm in diameter and 500 nm in height, were fabricated by nanoimprint using an intermediate polymer stamp (IPS), as shown in Fig. 1(a). The IPS was replicated from a nickel stamp with the imprint condition of 150 ℃ and 40 bar for 5 min, and coated with trichloro(1H,1H, 2H, 2H-prefluorooctyl)silane (FOTS) to promote stamp separation after imprint.

Next, a 4 μm thick photoresist was spin-coated onto the SU-8 nanopillars and soft-baked at 95 ℃ for 15 min. After ultra-violate (UV) exposure through a photomask and development, the patterned micropost array was created, as shown in Fig. 1(b). Reactive ion etching (RIE) (790 RIE system, Plasma-Thermal, USA) with a condition of 20/2 sccm SF_6/O_2, 10 mTorr, and 120 W RF power for 4 min was used to remove the nanopillars not covered by photoresist, as shown in Fig. 1(c). The photoresist was also used as an etch mask to etch the 2.7 μm diameter, 12 μm height Si microposts with a deep reactive ion etching (DRIE) system (LPX ICP LE0729, SPTS, UK). The etch condition was 138/11 sccm SF_6/O_2, 28 mTorr chamber pressure, 600 W coil power, and 14.8 W platen power at 13.56 MHz for 3.5 min, as shown in Fig. 1(d). After removing the photoresist, the thin residual layer from nanoimprint around the SU-8 nanopillars was removed by RIE with 20/2 sccm O_2/SF_6, 10 mTorr, and 120 W RF power for 2 min. Subsequently, the Si nanopillars on top of the microposts were formed by etching in the DRIE system with a condition of 70/35 sccm C_4F_4/SF_6, 10 mTorr chamber pressure, 600 W coil power, and 10 W platen power for 1.2 min. Finally, the SU-8 etch mask was removed in the RIE system using an O_2 plasma with 20 sccm O_2, 10 mTorr, and 100 W RF power for 5 min, as shown in Fig. 1(e). The Si mold was coated with FOTS as an anti-sticking layer, as shown in Fig. 1(f). PDMS (base:cross-linker weight ratio = 10:1, Sylgard 184, Dow Corning, USA) was poured onto the Si mold coated with FOTS and degassed in a vacuum chamber at 10^{-2} bar for 2 h. The negative mold was generated after curing at 25°C for 12 h and baking at 110°C for 15 min, and then coated with FOTS, as shown in Figs. 1(g-h).

As shown in Fig. 1(i), PDMS was spin-coated onto the negative mold and then degassed and baked as described earlier. Microposts with nanopillars were obtained after peeling the PDMS off the negative mold, cured at 25°C for 12 h, and baked at 110°C for 6 h, as shown in Fig. 1(j). A longer baking time was needed to form the microposts with nanopillars to ensure that PDMS was fully cured. The PDMS micropost array was treated in a critical point dryer (EM CPD300, Leica, Germany) after being ultrasonicated in 100% ethanol (Sigma-Aldrich, USA) for 1 min to prevent microposts sticking to one another. Micrograph of 2.7 μm diameter, 12 μm height, and 3.3 μm spacing microposts without nanopillars is shown in Fig. 1(k). Surface with nanopillars of 220 nm diameter, 500 nm height, and 280 nm spacing is shown in Fig. 1(l). In Fig. 1(m), similar nanopillars were fabricated on top of the 12 μm tall microposts. The microposts were in hexagonal arrangement with a 3.3 μm edge-to-edge spacing between two adjacent microposts. The traction force sensitivity of the PDMS micropost array depended on the micropost design including the height, diameter, and spacing of the micropost. Deep reaction ion etching technology was developed to form these tall microposts to achieve high sensitivity. The dry etching conditions were optimized to form tall microposts with small diameter. The spacing between the microposts was selected to ensure that the cells would stay on the top of the microposts while avoiding

stiction with adjacent microposts.[28] In addition, the dimensions of the nanopillars were chosen so that they would have significant influence on cell migration behavior.

Furthermore, microposts without nanopillars were fabricated using similar fabrication technology described above, as shown in Supplementary Figs. S1(a-g). On the other hand, microposts with silicon oxide or titanium oxide were formed by depositing silicon oxide or titanium oxide on top of the microposts using electron beam evaporation (ATS 500, HHV, UK), as shown in Supplementary Fig. S1(h). The silicon oxide and titanium oxide were deposited using 10 kV electron beam with deposition rate of 4.8 and 6.0 nm/min, respectively. The oxides deposited were directional since the evaporation was carried out at low pressure of 2×10^{-5} Torr, corresponding to a mean free path of 402 cm. Since the distance between the source and the sample was 35 cm, this ensured that the oxides were directionally deposited only on the top and the bottom of the microposts, and not on the sidewalls.[15,32] In addition, the temperature of the sample stage during the 4 min evaporation was kept at 45 °C by water cooling when 20 nm thick silicon oxide or titanium oxide was evaporated on top of the microposts. Thus, the effect of temperature on the mechanical properties of the microposts was negligible. Subsequently, these micropost sensing platforms were adhered onto the confocal dishes for further surface functionalization.

2.2 Surface treatment of micropost sensing platforms

In order to keep the cells on top of the microposts and avoid cells being trapped in between microposts, all the micropost arrays were coated with fibronectin (FN) on top of the microposts and 0.2% Pluronic F-127 (Sigma-Aldrich, USA) on the sidewalls of the microposts. Cells stayed on the FN coated top surface of microposts and did not migrate onto the micropost sidewalls as the Pluronic coating kept the cells away. To prepare such surface coating conditions for the micropost arrays, a FN coated PDMS pad was first generated. A $1\times1\times0.5$ cm^3 PDMS pad with a weight ratio of 20:1 was generated through curing on 110 °C hotplate for 1.5 h after degassing at 10^{-2} mbar vacuum chamber for 30 min. The PDMS pad was treated using an O_2 plasma with 135 sccm O_2, 15 sccm N_2, 150 mTorr, and 25 W RF power within a Faraday cage for 15 s and the water contact angle was measured to be 85° after the plasma treatment. 25 µl FN (50 µg/ml, Sigma-Aldrich, USA) was coated on the PDMS pad and kept at 4 °C for 4 h. The excess FN was removed by rinsing with DI water. After drying by N_2, this PDMS pad with FN coating was used to transfer FN to the top of microposts.

A plasma system (GIGAbatch 310 M, PVA TePla, Germany) was used to treat the micropost platform with an O_2 plasma using 135 sccm O_2, 15 sccm N_2, 150 mTorr, and 30 W RF power within a Faraday cage for 20 s. Subsequently, the FN-coated PDMS pad was used to contact the PDMS micropost platform for 1 min 30 s and transferred the FN to the top of microposts on the platform. Then the platform was immersed in 100% ethanol for easy separation of the PDMS pad from the microposts and the platform was ready for cell seeding.

The platform was immersed in 70% ethanol for disinfection and then rinsed twice with phosphate-buffered saline (PBS) in a biological safety cabinet. The micropost arrays were then labeled with a

lipophilic dye (DiI, 5 mg/ml in distilled water, 1,10-dioleyl-3,3,30,30-tetramethylindocarbocyanine methanesulfonate, Invitrogen, USA) by submerging the platform at 25 ℃ for 90 min. The red dye made it easier to analyze the micropost displacement caused by the cell traction force using the fluorescence signal. After rinsing in PBS three times, the platform was immersed in 0.2% Pluronic F-127 (Sigma-Aldrich, USA) and kept at 25 ℃ for 40 min to coat the micropost sidewalls with Pluronic. With FN coating on top and Pluronic on sidewalls of microposts, cells would migrate on top of the microposts and not adhere to the sidewall. Finally, the platform was rinsed thrice with PBS and submerged in PBS for cell culture and imaging.

2.3 Cell culture and seeding

MC3T3-E1 osteoblastic cells were obtained from American Type Culture Collection (ATCC numbers CRL-2594) and maintained in high glucose Dulbecco's modified eagle medium (DMEM, Invitrogen, USA), supplemented with 10% fetal bovine serum (FBS, Gibco, USA), antibiotic-antimycotic (100 units/ml of penicillin, 100 mg/ml of streptomycin, and 0.25 mg/ml of amphotericin B, Gibco, USA), and 2 mM alanyl-L-glutamine (Gibco, USA). Cells were incubated at 37 ℃ and 5% CO_2 with culture medium changed every 2 days. After washing the PDMS substrates with 70% alcohol once and PBS twice, the MC3T3-E1 cells were seeded at a density of 3×10^4 cells/cm^2. The culture dish was preserved at 37 ℃ in 5% CO_2 in an incubator for 6 h to allow the complete attachment of MC3T3-E1 cells on the designed platforms.

2.4 Cell migration trajectory, speed, and morphology analysis

The migration trajectory, speed, and morphology of MC3T3-E1 were analyzed using the time-lapse images. After cells attached and spread on the platform over 6 h, the medium was replaced by a CO_2-independent medium (Invitrogen 18045-088, USA), 10% FBS, and antibiotic-antimycotic, supplemented with 2 mM alanyl-L-glutamine (Gibco, USA) for time-lapse imaging. Images were captured every 5 min for 16 h using an upright microscope (Eclipse Ni-E, Nikon, Japan). A 20× objective lens was used, and cells were kept in an incubation chamber of 37 ℃. The cell migration behaviors were analyzed using the Manual Tracking plugin of Image J software. Cells that were alive, not divided, and had no interaction with other cells during the 16 h imaging period were analyzed. All the data were from at least 3 independent assays. Statistical analysis was performed using one-way analysis of variance (ANOVA) and Tukey's post hoc test.

2.5 Traction force analysis using bent microposts

Time-lapse images were captured using a Nikon microscope at a time interval of 3 min for 16 h. A 50× objective lens was used. Bright-field images were captured to show cell positions, and fluorescent images of the stained microposts were captured to acquire the bending displacement of microposts. The micropost sensing platforms consisted of micropost arrays with nanopillars or various coatings on top. The presence of nanopillars or coatings did not change the spring constant of micropost, hence the traction force sensing remained effective with the micropost array. This was verified by simulations using

the finite element analysis (FEA) suite (Multi-physics 5.4b, COMSOL, USA), as shown in Supplementary Fig. S2.[28,31] The results indicated that the fitted spring constant of 12.16 nN/μm for microposts without nanopillars, microposts with nanopillars, and microposts with oxide coatings was identical. The micropost displacement and spring constant were used to calculate the cell traction force using a custom-programmed MATLAB (R2010b, The MathWorks, USA) graphical user interface.[28]

2.6 Cell imaging using scanning electron microscopy

After time-lapse imaging, the cell culture medium in the dish was removed, and platform was washed twice with 1% PBS for 5 min each time. Then, cells were fixed with 4% paraformaldehyde for 15 min. After cell fixation, the platform was washed with 1% and 0.25% PBS each for 5 min, followed by rinsed twice in DI water for 10 min each. Subsequently, cells were dehydrated for 5 min each time using a series of increasing ethanol concentrations (30%, 50%, 70%, 80%, 95%, and 100%). Cells were dried using a critical point dryer, in which CO_2 was the transitional medium. A thin layer of gold was then sputter-coated on the platform using a thin film coater (Q150 coater, Quorum Technologies Ltd., UK). High-resolution images of the fixed cells were captured using a field emission scanning electron microscope (SEM) (SU5000 FE-SEM, Hitachi, Japan) with a 10 kV electron beam. These images were used to analyze the number and length of filopodia and long protrusions of cells. Typical filopodia were narrow with width of 200–400 nm and 4–30 μm long. Long protrusions had width larger than 400 nm, and protrusion length was defined as the distance between the edge of the cell membrane and the protrusion tip, and it could be 5–50 μm long.

3. Results And Discussion

3.1 Surface energy regulates cell responses

The physiochemical properties of ECM could have strong effects on cell-ECM interactions.[33] In this study, surfaces with flat PDMS, nanopillars, silicon oxide, and titanium oxide were developed, and their influence on cell migration behaviors was investigated. X-ray photoelectron spectroscopy (XPS) was used to study the chemical compositions of the oxides. The silicon oxide was in the form of $SiO_{1.7}$ and the titanium oxide was in the form of $TiO_{1.4}$ based on the XPS analysis.

Surface energy of an ECM or an engineered platform is related to its physical and chemical characteristics.[34] Water contact angle measurement was used to evaluate the surface energy of different surfaces on the microfabricated platforms. Figure 2 shows the water contact angle, migration trajectory, and cell morphology on different surfaces without FN coating. Surfaces with flat PDMS and nanopillars were hydrophobic (contact angle > 90°) with a larger water contact angle of 101° and 131°, corresponding to the low surface energy of 22.9 and 16.0 mN/m, respectively, as shown in Figs. 2(a-b). On the other hand, PDMS surfaces coated with 20 nm thick silicon oxide or titanium oxide were hydrophilic (contact angle < 90°). Their water contact angles were 12° and 74°, respectively, and the corresponding surface energy was 47.8 and 32.3 mN/m, as shown in Figs. 2(c-d). Surface energy of biomaterial could drive

ligand topology and generate different focal adhesion signaling pathways between cells and substrates. These signals could modulate cytoskeletal tension and cause different cell responses.[35]

To observe the difference in cell behavior, the Supplementary movie SV1 of MC3T3-E1 cell migration on different surfaces over 16 h with 5 min/frame were given. As shown in Figs. 2(e-h), cells cultured on these surfaces had random migration trajectories. No guidance effect for cells on various platforms was found as cells had similar migration speed in the x- and y-directions, as shown in Supplementary Fig. S3(a). This is due to the lack of directional surface topography for cell migration guidance. However, cells migrated on hydrophobic flat PDMS or nanopillar surfaces had longer paths and faster movements than those cells on hydrophilic oxide surfaces. The persistence length and kymographs of cell migration on different surfaces were analyzed to characterize the total travel distance of the migration path and the pace of the cell movement, as shown in Supplementary Figs. S4 and S5. Cells migrated on PDMS surface with nanopillars had the longest total migration path and the fastest cell movement pace. These could be related to the PDMS surface with nanopillars was the most hydrophobic surface, which made it easiest for cells to detach from the surface and continue to migrate. Both the persistent lengths and the kymographs are consistent with the trajectories shown in Figs. 2(e-h). Figures 2(i-l) show the distinctive morphologies of MC3T3-E1 cells on different surfaces. Cells cultured on hydrophobic flat PDMS or nanopillar surfaces possessed polarized morphologies, and the elongated cells had leading and trailing edges, indicating strong motile behavior as shown in Figs. 2(i-j). In particular, the presence of nanotopography can promote cell elongation, contraction, and ultimately cell migration. As shown in Fig. 2(j), nanopillars formed discontinuous surface for cell adhesion. This made it easier for cells to attach to and detach from the surface during migration, leading to rapid cell movement.[36] Furthermore, deformation of the nanopillars was observed, suggesting that the nanopillars may be more conducive to transmitting cytoskeletal tension to the substrate.[37] On surface with nanopillars, cells extended numerous filopodia in all directions and the extensions of filopodia were more prominent around the advancing cell edge. However, cells grown on hydrophilic oxide surfaces showed less elongation and more spreading, as shown in Figs. 2(k-l). One plausible explanation for these differences is related to the surface energy modulation of the distribution and deposition of adsorbed proteins.[38] These results indicate that surface energy could be a critical factor affecting cell migration behaviors and cell shapes.

3.2 Cell migration and cell morphology on different surfaces

Figure 3 shows the cell migration speed, aspect ratio, and elongation of MC3T3-E1 cells on different surfaces without FN coating. Cells migrated fastest at 0.99 μm/min on surface with nanopillars, as shown in Fig. 3(a). In addition, cells on flat PDMS surface migrated faster with a speed of 0.64 μm/min than those on silicon oxide or titanium oxide surfaces. The migration speed of cells on the silicon oxide surface was 0.36 μm/min compared to 0.25 μm/min on the titanium oxide surface. These results agree with previous studies that cell migration speed was closely related to surface topography, surface energy, and surface chemistry.[39] Interestingly, cells on nanopillars had the highest migration speed compared to other surfaces. This is attributed to the fact that nanopillars generated a most hydrophobic surface,

making it more difficult to form focal adhesion sites, and hence weaker cell adhesion and faster cell migration speed.[40] On the contrary, hydrophilic surfaces promoted stronger cell adhesion, and resulted in slower cell migration speed. However, a highly hydrophilic surface inhibited the binding of cell adhesion mediators, thus hindering cell adhesion behavior. The moderate hydrophilic surface with a contact angle between 60° to 80° has been shown to have the highest cell adhesion.[23,41,42] On titanium oxide surface, the water contact angle was 74°, corresponding to the highest cell adhesion and the slowest migration speed.[17]

Changes in aspect ratio over 16 h are shown in Fig. 3(b). The cell aspect ratio is defined as the ratio between the major and minor axes when cells are fitted to an ellipse.[10] Initially, cells on the flat PDMS surface had a more rounded shape, and the aspect ratio was small because of the unstable attachment to the hydrophobic PDMS surface.[23] Once cells formed a stable attachment to the PDMS surface over time, the aspect ratio increased with time. It became larger than those on the titanium oxide surface after 9 h. For cells on the surface with nanopillars, they also were more rounded initially, and the aspect ratio increased with time. However, cells had a smaller aspect ratio but frequent cytoskeletal rearrangement compared to those on flat PDMS surface, corresponding to more rapid cell movement, as shown in Supplementary movie SV1(b).[43] In addition, the aspect ratio for cells on titanium oxide surface was larger than those on silicon oxide surface.

Furthermore, cell elongation was obtained by averaging the aspect ratio over 16 h, as shown in Fig. 3(c). MC3T3-E1 cells on the surface with nanopillars showed a cell elongation of 3.65, similar to those on the flat PDMS surface with an elongation of 3.82. In comparison, cell elongation for cells seeded on silicon oxide and titanium oxide surfaces was 2.90 and 3.48, respectively. These results indicated that the polarization characteristics of cells on the hydrophobic surface were more obvious than those on the hydrophilic surface. This may be due to the different surface energy that affected the distribution of adsorbed protein, and proteins on the hydrophobic surface were more likely to form unidirectional distribution.[18,38] The elongation of cells on nanopillars was similar to that on flat PDMS surface, as they had similar surface energy and fast cytoskeletal rearrangement. However, there was still significant difference compared with cells on silicon oxide surface, which had a more rounded shape. The hydrophilic silicon oxide had the highest surface energy, making it easier for cells to adhere on the surface in multiple directions, resulting in less cell elongation. These results showed that cell morphology could be controlled by changing the surface energy.

On the other hand, cell area on silicon oxide or titanium oxide surfaces was larger than on flat PDMS or nanopillar surfaces, as shown in Supplementary Fig. S3(b). These findings coincided with the previous finding that the fibroblast cells on hydrophilic surfaces exhibited larger cell area compared to those on hydrophobic surfaces.[23] In particular, cells on nanopillar surface showed the smallest cell area, which was consistent with a previous report that indicated cells on nanopillars resulted in a 40–50% reduction in cell area compared to those on a flat surface.[44] These results indicate that there are close relationships between cell migration speed, morphology, and surface energy on different surfaces.

3.3 Cell migration behaviors influenced by fibronectin coating

The migration behavior and cell morphology for cells on different surfaces coated with FN were further investigated, as FN coating on top of the microposts was needed for traction force study. All the work on cell migration characterization from this point on was carried out on surfaces coated with FN. With FN coated on the surfaces, the water contact angles of flat PDMS, nanopillars, silicon oxide, and titanium oxide were 64°, 82°, 22°, and 38°, respectively, as shown in Supplementary Fig. S6. The contact angles of these surfaces decreased, which corresponded to the increases in surface energy. The cell migration speed decreased on all surfaces coated with FN, but the trend remained unchanged, as shown in Fig. 4(a). A migration speed of 0.78 μm/min was obtained for cells on nanopillars with FN coating, which is significantly higher than other FN coated surfaces. In addition, the cell migration speed on flat PDMS was 0.43 μm/min, and it is higher than on silicon oxide and titanium oxide, which had migration speed of 0.37 and 0.33 μm/min, respectively. On the other hand, cell aspect ratio and elongation had little dependence on surface conditions, as shown in Figs. 4(b-c). With FN coating, cell morphology was similar on all surfaces, except for cells on nanopillars which showed a slightly larger aspect ratio.

After the FN coating, all surfaces became more hydrophilic and cell adhesion was enhanced, resulting in reduced cell migration speed. Furthermore, the addition of the protein layer facilitated cell spreading in multiple directions, leading to more rounded cell shape. These results may be related to the surface energy-driven ligand assembly.[35] Cell migration behavior changed due to variations in protein adsorption.[45,46] Additionally, FN is a major component of ECM that mediates various cellular behaviors. When cells attach to the ECM surface, focal adhesions are formed by binding of the integrin receptors to FN adsorbed on the surface, constituting a mechanotransduction link between the cytoskeleton and the ECM.[9] The actin cytoskeleton mediates tension to adapt its shape and exhibits complex mechanocoupling responses to achieve cell migration. The formation of focal adhesions is the prerequisite for the generation of cell traction force. Cell adhesion area, protein adsorption, and fibrilar adhesion are changed and thus influence the complex cell force that acts on the ECM surface. Surface energy-driven mechanotransduction may cause cells to migrate faster on surface with nanopillars coated with FN.

3.4 Cell traction force exerted on microposts with nanopillars or oxide coatings

In this study, micropost sensing arrays were used to measure the cell traction force on platforms with various surface conditions. All the micropost arrays were coated with FN on top and Pluronic on the sidewalls of microposts, as these coatings were necessary to keep the cells on top of the microposts for cell traction force study. Supplementary Fig. S7 shows that the cell migration speed on flat PDMS surface and on microposts without nanopillars had no significant difference. Since cell migration on flat PDMS

surface and on microposts without nanopillars was similar, the micropost arrays could be applied to sense the cell traction force.

Figure 5. Traction force development for MC3T3-E1 cell migration on PDMS microposts (a) without and (b) with nanopillars. (c) Normalized traction force in leading, middle, and trailing regions of cells on microposts with various surface conditions. Microposts were coated with FN on top and Pluronic on sidewalls. The yellow dashed line indicates cell contour. The starting and ending positions are indicated by asterisks and dots in the micrographs, respectively. The white arrows indicate the traction force on microposts. The length of the white arrow represents the magnitude of the traction force. Cell migration direction is marked by a blue arrow, representing the movement of the cell centroid during a single migration cycle. One-way ANOVA and Tukey's post hoc test, ***$p < 0.001$.

As shown in Fig. 5(a), the measured traction force was directed towards the cell center with higher force acted around the cell periphery and lower force at the cell center. During migration, the cell elongated by protruding the leading and trailing regions. The corresponding traction force increased gradually, and higher force was found near the leading region compared to the trailing region of the cell. The cell barely moved forward when it was elongated. Then, the trailing region detached from the microposts, and the traction force dropped in both the leading and trailing regions. As the trailing region retracted, the cell moved forward and started the migration cycle again. This cyclic behavior repeated itself during cell migration and is consistent with previous findings.[28,29] As shown in Fig. 5(b), cells migrated on microposts with nanopillars had the similar cyclic behavior but showed greater amplitudes of traction force in all three cell regions and shorter cycle time. Meanwhile, microposts with silicon oxide or titanium oxide also had the similar cyclic behavior. However, cells migrated with lower amplitudes of traction force and longer cycle time. These results indicate that cell migration was cyclic, and shorter cycle time and higher migration speed corresponded to cell migration on surface with larger traction force. In addition, cells generated larger traction force when they were elongated compared to contracted cells, which may be due to the greater actin cytoskeleton tension during cell elongation. Being able to realize the traction force distribution for cells during migration will provide a better understanding of the cell migration mechanisms.

Figure 5(c) shows the normalized net traction force in the leading, middle, and trailing regions when cells were elongated. For cells seeded on microposts without nanopillars, the traction force exerted in the leading region was 9.9 ± 0.7 nN, higher than 5.8 ± 0.6 nN in the trailing region and 3.44 ± 0.6 nN in the middle region. The trend of traction force generally agrees with previous reports.[28,29] In comparison, the traction force of the leading, middle, and trailing regions for cells seeded on microposts with nanopillars was larger than that on microposts without nanopillars. The traction force in the leading region was 17.1 ± 1.0 nN, 10.2 ± 0.9 nN in the trailing region, and 6.8 ± 0.5 nN in the middle region. On the other hand, the traction force of cells on silicon oxide surface was smaller in the leading (8.4 ± 0.4 nN), middle (2.8 ± 0.3 nN), and trailing (5.7 ± 0.4 nN) regions when compared with cells on the flat PDMS surface. For cells on titanium oxide surface, the traction force in the leading, middle, and trailing regions was 7.2 ± 0.4, 2.4 ± 0.3, and 5.1 ± 0.4 nN, respectively, and they were smaller than cells on the silicon oxide surface.

In general, cells on all surfaces had a large force imbalance from the leading to trailing regions. Traction force of the leading region was the largest, and the middle region was the smallest. Furthermore, the force in the leading region was greater than that in the trailing region when cells were moving forward. This may be due to the fact that more filopodia were in the leading region compared to the trailing region, which was related to the ligand adhesion that formed a larger fibrilar adhesion force. On the other hand, cells on various surfaces had traction forces with different magnitude, which corresponded to the related cell migration speed. Cells on the nanopillars had the largest traction force, which corresponded to the fastest migration speed. With the introduction of nanotopography, nanopillars could absorb protein easily, which facilitated the transmission of traction force to the substrate.[47] Also, nanopillars could promote the formation and extension of filopodia and long protrusions, therefore the fibrillar adhesion force between the cells and the substrate could be enhanced. Hence, it can be inferred that strong fibrillar adhesion force as well as good transmission of traction force could result in large cell traction force and high migration speed on surface with nanopillars.[48]

3.5 Cells migrated on microposts with nanopillars have more filopodia and long protrusions

Figure 6 shows the distinctive morphologies of MC3T3-E1 cells on different platforms and the quantitative analysis of filopodia and long protrusions. Cells attached to the top of microposts due to the selectively coated proteins on top and Pluronic F-127 on the sidewall of microposts.[31] As cells migrated, microposts bent under cell traction force, and the displacement of microposts served to quantify the traction force exerted by the cells. As shown in Fig. 6(a), cells on microposts without nanopillars bent the microposts towards the cell center due to cell traction force, similar to cells migrated on top of microposts with nanopillars, as shown in Fig. 6(b). In addition, microposts with silicon oxide or titanium oxide bent in similar manners as shown in Figs. 6(a-b). However, cells on microposts with nanopillars had more filopodia and long protrusions, which was consistent with our previous findings that nanostructures promote the generation of filopodia and long protrusions.[19]

High-resolution SEM was utilized to quantify the number and length of filopodia and long protrusions on different platforms, as shown in Figs. 6(c-d) and Supplementary Figs. S8(a-b). The MC3T3-E1 cells on microposts without nanopillars typically had 6 filopodia/cell and 4 long protrusions/cell. For cells on microposts with silicon oxide and titanium oxide, the numbers of long protrusions were 3 and 4, respectively, and the same number of 5 filopodia/cell. For cells on microposts with nanopillars, the numbers of filopodia/cell and long protrusions/cell were 13 and 6, respectively. More filopodia and long protrusions were formed on microposts with nanopillars on top, which resulted in the larger cell traction force. However, there is no significant difference in the length of filopodia or long protrusions, as shown in Supplementary Figs. S8(a-b). Since the microposts were separated from one another, the discontinuous gaps between the microposts may limit the extensions of filopodia and long protrusions. Having more filopodia and long protrusions extended from the cell membrane resulted in a larger traction force, and thus gave rise to the higher migration speed of MC3T3-E1 cells on nanopillars.[19] These results agreed

with previous observations that more actin-rich protrusions from cell edges generated larger contractile forces during cell migration.[49]

3.6 Dynamic traction force monitored on various surfaces

During directional migration, cells will undergo cyclic dynamic changes during which the distribution of cell traction force from the leading front to the trailing edge can affect the cell migration.[50] Thus, the measurement of cell traction force development over time from the leading to the trailing regions during cell migration is essential to provide insights into cell migration dynamics. Using the force vectors measured by the microposts and normalizing the force by the number of microposts covered by a cell, the cell traction force in the three regions and cell migration speed were analyzed as a function of time, as shown in Figs. 7(a-d).

Figure 7(a) shows that cells migrating on microposts without nanopillars contracted initially at 0 min with a relatively smaller traction force for all regions. Over time, the cells became elongated with increased traction force. Traction force of the leading region was larger than that of the trailing region, and traction force of the middle region was the lowest. The trailing region started to release at 69 min as the traction force dropped in both the leading and trailing regions. After the trailing region was completely disconnected from the microposts at 81 min, cells contracted, and the next migration cycle began. The cyclic changes in the traction force and cell morphology agree with our previous findings.[28] When cell shape changed from contraction to elongation, lamellipodia protruded over time and formed leading, middle, and trailing regions. Traction force increased gradually when the cell was elongated, but the cell barely moved. Cell speed increased significantly after the adhesive sites in the trailing region released, and the cell moved forward. Then the next cell migration cycle started, and the change of speed repeated.

For cells migrating on microposts with nanopillars, silicon oxide, and titanium oxide, the time dependent traction force had similar cyclic changes as cells on microposts without nanopillars, as shown in Figs. 7(b-d). The traction force for cells on microposts with nanopillars increased gradually with the protrusion of the leading region, and the cell shape changed from contracted to elongated. Traction force increased significantly when the cell changed from contraction to elongation. Later, traction force dropped rapidly as the trailing region was released, and the cell moved forward, completing the cytoskeleton reorganization. Compared with the other three surfaces, surface with nanopillars generated larger traction force, probably related to the rapid skeletal reorganization of the cells on nanostructures as mentioned above. With the release of the trailing region, cell speed increased as the cell moved ahead. A skeleton reorganization cycle was defined as the time needed between two consecutive maximum instantaneous speeds. This cycle time of the cells on the microposts with nanopillars was 42 min, and 54, 63, and 66 min for microposts without nanopillars, with silicon oxide, and with titanium oxide, respectively. These results showed that cells had the shortest cycle time on the microposts with nanopillars.

Furthermore, as shown in Fig. 7, the maximum instantaneous speed was 1.75, 1.66, 1.05, and 0.87 μm/min for microposts without nanopillars, microposts with nanopillars, microposts with silicon oxide,

and microposts with titanium oxide, respectively. The corresponding traction force was 12.08, 11.62, 7.15, and 6.98 nN for these four types of micropost surfaces, respectively. To a certain extent, the maximum instantaneous speed was higher for larger traction force. In addition, the dynamic cell traction force on microposts with nanopillars was the largest throughout the cell migration cycle compared to the other three surfaces. The larger dynamic traction force also correlated to a higher migration speed. It is evident that dynamic traction force is a function of surface topography and coating that can strongly influence cell migration. Using micropost arrays to monitor cell traction force, cells on various surfaces showed similar time dependent traction force changes during migration. However, the magnitude of the cell traction force depended on the surface topography and coating on the micropost surface. These results had potential implications for designing biomimetic ECM in bone tissue engineering.

4. Conclusions

In this paper, various surface topographies and coatings, including flat PDMS, nanopillar, silicon oxide, and titanium oxide surfaces, were developed to study their effects on cell migration behaviors. Surfaces with flat PDMS or nanopillars were hydrophobic, while surfaces coated with silicon oxide or titanium oxide were hydrophilic. The results were related to cell migration speed and changes in cell morphology, including cell aspect ratio, elongation, and area, due to the changes in surface energy. Cells on hydrophobic surfaces with lower surface energy showed higher migration speed, larger cell elongation, and less cell spreading than those on hydrophilic surfaces with higher surface energy. Cells migrated fastest with 0.99 μm/min on nanopillar surface and slowest with 0.25 μm/min on titanium oxide surface. Furtherly, the effects of protein coating on cell migration behaviors were analyzed. The cell migration speed on nanopillars with FN coating was 0.78 μm/min, which was still significantly different from cells on other surfaces with FN coating. The different migration speed may be related to the dependence of FN adsorption on different surfaces that have different surface energies.

PDMS micropost sensing platforms with various topographies and coatings were used to study cell traction force over time to correlate traction force development with surface conditions and migration behaviors. Cells migrated on microposts with nanopillars had cyclic behaviors and formed the largest traction force on the microposts than cells migrating on microposts without nanopillars. For cells elongated on microposts with nanopillars, the traction force was larger in the leading (17.1 nN), middle (6.75 nN), and trailing (10.2 nN) regions compared to cells on the flat PDMS surface with traction force of 9.9, 3.4, and 5.8 nN in the leading, middle, and trailing regions. More filopodia/cell and long protrusions/cell were observed for the cells on microposts with nanopillars compared to those on microposts without nanopillars, corresponding to the higher traction force and faster migration speed. To the best of our knowledge, this is the first study to analyze the dynamic cell traction force on different surfaces using micropost arrays. These results provide a better understanding of cell migration on surfaces with various topographies and coatings, which could be valuable in developing smart bionic platforms for regenerative medicine.

Declarations

Conflict of Interests

There are no conflicts to declare.

Acknowledgements

This work was supported by the Center for Biosystems, Neuroscience, and Nanotechnology (CBNN) of City University of Hong Kong (9360148, 9380062), the University Grants Council of Hong Kong (GRF Projects: 11212519, 11207620, and 11207821). We gratefully acknowledge members of CBNN and cleanroom technical staff for their help.

Author Contributions

SWP conceived the project and designed the study. YC fabricated stamps, performed the experiments, analyzed the data, and wrote the original manuscript. SWP provided supervision, resources, data analysis, and manuscript revisions.

References

1. Rahmati, M., Silva, E. A., Reseland, J. E., C, A. H. & Haugen, H. J. Biological responses to physicochemical properties of biomaterial surface. *Chem Soc Rev* **49**, 5178-5224, doi:10.1039/d0cs00103a (2020).
2. Biazar, E., Kamalvand, M. & Avani, F. Recent advances in surface modification of biopolymeric nanofibrous scaffolds. *International Journal of Polymeric Materials and Polymeric Biomaterials*, 1-20, doi:10.1080/00914037.2020.1857383 (2021).
3. Cao, B., Peng, Y., Liu, X. & Ding, J. Effects of functional groups of materials on nonspecific adhesion and chondrogenic induction of mesenchymal stem cells on free and micropatterned surfaces. *ACS Appl Mater Interfaces* **9**, 23574-23585, doi:10.1021/acsami.7b08339 (2017).
4. Rashidi, H., Yang, J. & Shakesheff, K. M. Surface engineering of synthetic polymer materials for tissue engineering and regenerative medicine applications. *Biomater Sci* **2**, 1318-1331, doi:10.1039/c3bm60330j (2014).
5. Tsang, C. M. *et al.* Integration of biochemical and topographic cues for the formation and spatial distribution of invadosomes in nasopharyngeal epithelial cells. *Acta Biomater* **101**, 168-182, doi:10.1016/j.actbio.2019.10.043 (2020).
6. Xu, Y. & Pang, S. W. Natural killer cell migration control in microchannels by perturbations and topography. *Lab Chip* **19**, 2466-2475, doi:10.1039/c9lc00356h (2019).
7. Tang, Y. *et al.* TGF-beta1-induced migration of bone mesenchymal stem cells couples bone resorption with formation. *Nat Med* **15**, 757-765, doi:10.1038/nm.1979 (2009).

8. Ermis, M., Antmen, E. & Hasirci, V. Micro and Nanofabrication methods to control cell-substrate interactions and cell behavior: A review from the tissue engineering perspective. *Bioact Mater* **3**, 355-369, doi:10.1016/j.bioactmat.2018.05.005 (2018).
9. van Helvert, S., Storm, C. & Friedl, P. Mechanoreciprocity in cell migration. *Nat Cell Biol* **20**, 8-20, doi:10.1038/s41556-017-0012-0 (2018).
10. Tang, Q. Y. *et al.* Influence of engineered surface on cell directionality and motility. *Biofabrication* **6**, 015011, doi:10.1088/1758-5082/6/1/015011 (2014).
11. Park, J. *et al.* Directed migration of cancer cells guided by the graded texture of the underlying matrix. *Nat Mater* **15**, 792-801, doi:10.1038/nmat4586 (2016).
12. Wu, J. *et al.* Directional migration of vascular smooth muscle cells guided by synergetic surface gradient and chemical pattern of poly(ethylene glycol) brushes. *Journal of Bioactive and Compatible Polymers* **28**, 605-620, doi:10.1177/0883911513506665 (2013).
13. Zhou, S. F. *et al.* A Unidirectional Cell Switching Gate by Engineering Grating Length and Bending Angle. *PLoS One* **11**, e0147801, doi:10.1371/journal.pone.0147801 (2016).
14. Tang, Q. Y. *et al.* Control of cell migration direction by inducing cell shape asymmetry with patterned topography. *J Biomed Mater Res A* **103**, 2383-2393, doi:10.1002/jbm.a.35378 (2015).
15. Zhu, S., Eldeeb, M. A. & Pang, S. W. 3D nanoplasmonic biosensor for detection of filopodia in cells. *Lab Chip* **20**, 2188-2196, doi:10.1039/d0lc00173b (2020).
16. Refaaq, F. M., Chen, X. & Pang, S. W. Effects of topographical guidance cues on osteoblast cell migration. *Sci Rep* **10**, 20003, doi:10.1038/s41598-020-77103-0 (2020).
17. Ranella, A., Barberoglou, M., Bakogianni, S., Fotakis, C. & Stratakis, E. Tuning cell adhesion by controlling the roughness and wettability of 3D micro/nano silicon structures. *Acta Biomater* **6**, 2711-2720, doi:10.1016/j.actbio.2010.01.016 (2010).
18. Zhukova, Y. *et al.* The Role of Titanium Surface Nanostructuring on Preosteoblast Morphology, Adhesion, and Migration. *Adv Healthc Mater* **6**, doi:10.1002/adhm.201601244 (2017).
19. Cheng, Y., Zhu, S. & Pang, S. W. Directing osteoblastic cell migration on arrays of nanopillars and nanoholes with different aspect ratios. *Lab Chip* **21**, 2206-2216, doi:10.1039/d1lc00104c (2021).
20. Rapp, C., Baumgärtel, A., Artmann, L., Eblenkamp, M. & Asad, S. S. Open air plasma deposited antimicrobial SiOx/TiOx composite films for biomedical applications. *Current Directions in Biomedical Engineering* **2**, 43-47, doi:10.1515/cdbme-2016-0013 (2016).
21. Peters, R. J. B. *et al.* Silicon dioxide and titanium dioxide particles found in human tissues. *Nanotoxicology* **14**, 420-432, doi:10.1080/17435390.2020.1718232 (2020).
22. Syromotina, D. S. *et al.* Surface wettability and energy effects on the biological performance of poly-3-hydroxybutyrate films treated with RF plasma. *Mater Sci Eng C Mater Biol Appl* **62**, 450-457, doi:10.1016/j.msec.2016.01.075 (2016).
23. Wei, J. *et al.* Adhesion of mouse fibroblasts on hexamethyldisiloxane surfaces with wide range of wettability. *J Biomed Mater Res B Appl Biomater* **81**, 66-75, doi:10.1002/jbm.b.30638 (2007).

24. Basoli, F. *et al.* Biomechanical Characterization at the Cell Scale: Present and Prospects. *Front Physiol* **9**, 1449, doi:10.3389/fphys.2018.01449 (2018).
25. Capozza, R. *et al.* Cell Membrane Disruption by Vertical Micro-/Nanopillars: Role of Membrane Bending and Traction Forces. *ACS Appl Mater Interfaces* **10**, 29107-29114, doi:10.1021/acsami.8b08218 (2018).
26. Yang, Y., Wang, K., Gu, X. & Leong, K. W. Biophysical Regulation of Cell Behavior-Cross Talk between Substrate Stiffness and Nanotopography. *Engineering (Beijing)* **3**, 36-54, doi:10.1016/J.ENG.2017.01.014 (2017).
27. Plotnikov, S. V., Pasapera, A. M., Sabass, B. & Waterman, C. M. Force fluctuations within focal adhesions mediate ECM-rigidity sensing to guide directed cell migration. *Cell* **151**, 1513-1527, doi:10.1016/j.cell.2012.11.034 (2012).
28. Hui, J. & Pang, S. W. Dynamic Tracking of Osteoblastic Cell Traction Force during Guided Migration. *Cell Mol Bioeng* **11**, 11-23, doi:10.1007/s12195-017-0514-7 (2018).
29. Hui, J. & Pang, Stella W. Cell traction force in a confined microenvironment with double-sided micropost arrays. *RSC Advances* **9**, 8575-8584 (2019).
30. Li, Z. *et al.* Cellular traction forces: a useful parameter in cancer research. *Nanoscale* **9**, 19039-19044, doi:10.1039/c7nr06284b (2017).
31. Yang, M. T., Fu, J., Wang, Y. K., Desai, R. A. & Chen, C. S. Assaying stem cell mechanobiology on microfabricated elastomeric substrates with geometrically modulated rigidity. *Nat Protoc* **6**, 187-213, doi:10.1038/nprot.2010.189 (2011).
32. Wi, J. S. *et al.* Facile three-dimensional nanoarchitecturing of double-bent gold strips on roll-to-roll nanoimprinted transparent nanogratings for flexible and scalable plasmonic sensors. *Nanoscale* **9**, 1398-1402, doi:10.1039/c6nr08387k (2017).
33. Feller, L. *et al.* Cellular responses evoked by different surface characteristics of intraosseous titanium implants. *Biomed Res Int* **2015**, 171945, doi:10.1155/2015/171945 (2015).
34. Xiao, B. *et al.* Surface Modification and Charge Injection in a Nanocomposite Of Metal Nanoparticles and Semiconductor Oxide Nanostructures. *Sci Rep* **10**, 4743, doi:10.1038/s41598-020-58308-9 (2020).
35. Razafiarison, T. *et al.* Biomaterial surface energy-driven ligand assembly strongly regulates stem cell mechanosensitivity and fate on very soft substrates. *Proc Natl Acad Sci U S A* **115**, 4631-4636, doi:10.1073/pnas.1704543115 (2018).
36. Viela, F., Granados, D., Ayuso-Sacido, A. & Rodríguez, I. Biomechanical Cell Regulation by High Aspect Ratio Nanoimprinted Pillars. *Advanced Functional Materials* **26**, 5599-5609, doi:10.1002/adfm.201601817 (2016).
37. Maruthamuthu, V., Sabass, B., Schwarz, U. S. & Gardel, M. L. Cell-ECM traction force modulates endogenous tension at cell-cell contacts. *Proc Natl Acad Sci U S A* **108**, 4708-4713, doi:10.1073/pnas.1011123108 (2011).

38. Le Clainche, C. & Carlier, M. F. Regulation of actin assembly associated with protrusion and adhesion in cell migration. *Physiol Rev* **88**, 489-513, doi:10.1152/physrev.00021.2007 (2008).
39. Rostam, H. M., Singh, S., Vrana, N. E., Alexander, M. R. & Ghaemmaghami, A. M. Impact of surface chemistry and topography on the function of antigen presenting cells. *Biomater Sci* **3**, 424-441, doi:10.1039/c4bm00375f (2015).
40. Jenkins, T. L. & Little, D. Synthetic scaffolds for musculoskeletal tissue engineering: cellular responses to fiber parameters. *NPJ Regen Med* **4**, 15, doi:10.1038/s41536-019-0076-5 (2019).
41. Cavalcanti-Adam, E. A., Aydin, D., Hirschfeld-Warneken, V. C. & Spatz, J. P. Cell adhesion and response to synthetic nanopatterned environments by steering receptor clustering and spatial location. *HFSP J* **2**, 276-285, doi:10.2976/1.2976662 (2008).
42. Fokkelman, M. *et al.* Cellular adhesome screen identifies critical modulators of focal adhesion dynamics, cellular traction forces and cell migration behaviour. *Sci Rep* **6**, 31707, doi:10.1038/srep31707 (2016).
43. Hiraiwa, T., Yamada, T. G., Miki, N., Funahashi, A. & Hiroi, N. Activation of cell migration via morphological changes in focal adhesions depends on shear stress in MYCN-amplified neuroblastoma cells. *J R Soc Interface* **16**, 20180934, doi:10.1098/rsif.2018.0934 (2019).
44. Hu, W., Crouch, A. S., Miller, D., Aryal, M. & Luebke, K. J. Inhibited cell spreading on polystyrene nanopillars fabricated by nanoimprinting and in situ elongation. *Nanotechnology* **21**, 385301, doi:10.1088/0957-4484/21/38/385301 (2010).
45. Comelles, J., Estevez, M., Martinez, E. & Samitier, J. The role of surface energy of technical polymers in serum protein adsorption and MG-63 cells adhesion. *Nanomedicine* **6**, 44-51, doi:10.1016/j.nano.2009.05.006 (2010).
46. Zhou, K. *et al.* Effect of surface energy on protein adsorption behaviours of treated CoCrMo alloy surfaces. *Applied Surface Science* **520**, doi:10.1016/j.apsusc.2020.146354 (2020).
47. Lin, M. *et al.* Adsorption force of fibronectin controls transmission of cell traction force and subsequent stem cell fate. *Biomaterials* **162**, 170-182, doi:10.1016/j.biomaterials.2018.01.036 (2018).
48. Hou, Y. *et al.* Surface Roughness and Substrate Stiffness Synergize To Drive Cellular Mechanoresponse. *Nano Lett* **20**, 748-757, doi:10.1021/acs.nanolett.9b04761 (2020).
49. Eschenbruch, J. *et al.* From Microspikes to Stress Fibers: Actin Remodeling in Breast Acini Drives Myosin II-Mediated Basement Membrane Invasion. *Cells* **10**, doi:10.3390/cells10081979 (2021).
50. Trepat, X., Chen, Z. & Jacobson, K. Cell migration. *Compr Physiol* **2**, 2369-2392, doi:10.1002/cphy.c110012 (2012).

Figures

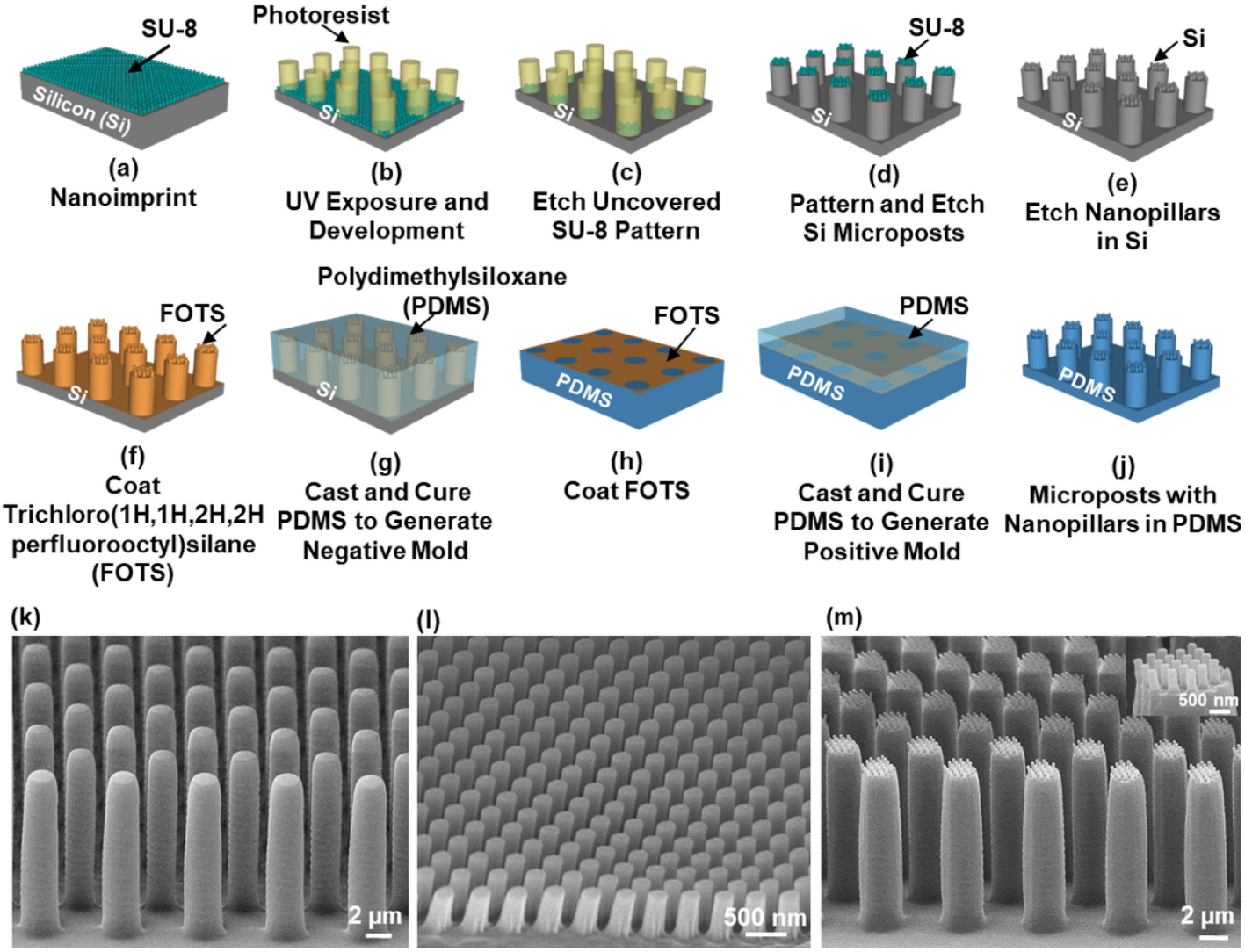

Figure 1

Schematics of fabrication technology for microposts with nanopillars. (a) Imprint SU-8 with simultaneous thermal and UV exposure. (b) UV lithography to pattern nanopillar array. (c) Reactive ion etching in SF_6/O_2 to remove uncovered SU-8 pattern. (d) Deep reactive ion etching (DRIE) of Si to form micropost array and remove photoresist. (e) Remove residual layer of SU-8 nanopillars and DRIE of Si to form nanopillar array, and remove SU-8 using plasma etching. (f-j) Double cast PDMS to generate desired patterns. Trichloro(1H,1H,2H,2H perfluorooctyl)silane (FOTS) was used as anti-sticking layer to promote easy demolding. Micrographs of (k) microposts without nanopillars, (l) surface with nanopillars, and (m) microposts with nanopillars.

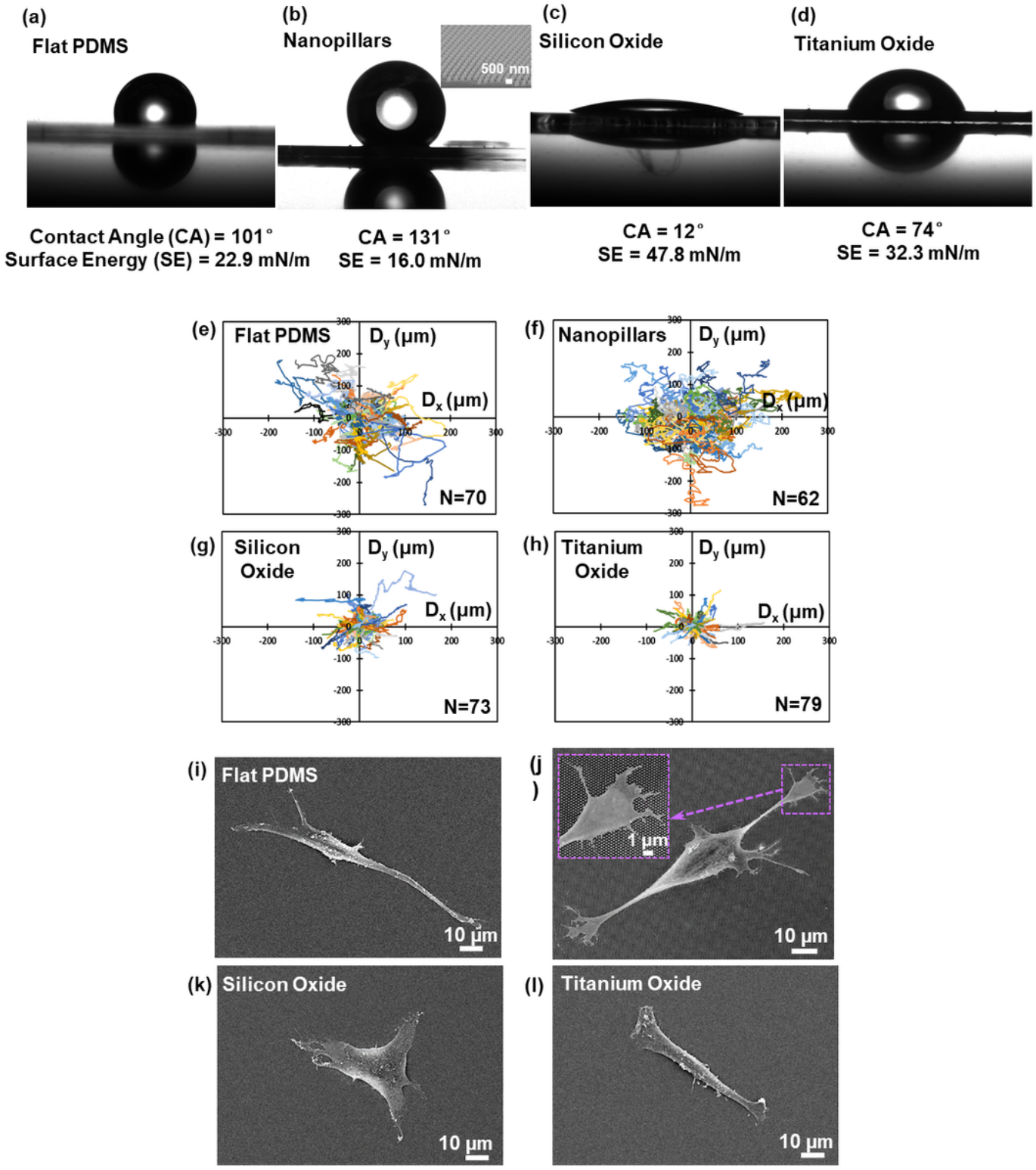

Figure 2

All surfaces without FN coating. Surface energy of (a) flat PDMS, (b) nanopillars, (c) silicon oxide, and (d) titanium oxide surfaces. Migration trajectories of MC3T3-E1 cells on (e) flat PDMS, (f) nanopillars, (g) silicon oxide, and (h) titanium oxide surfaces. Micrographs of cells on (i) flat PDMS, (j) nanopillars, (k) silicon oxide, and (l) titanium oxide surfaces.

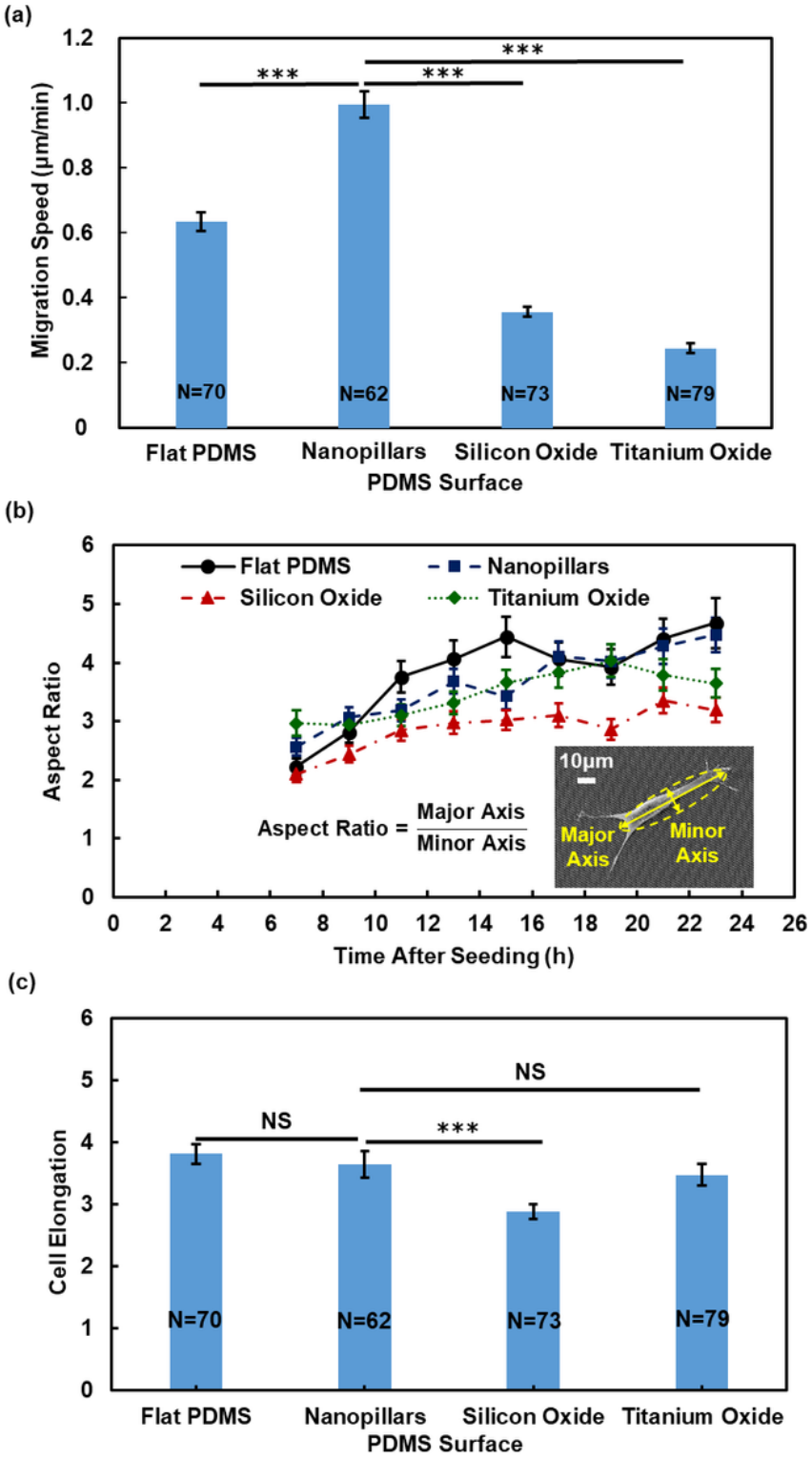

Figure 3

All surfaces without FN coating. (a) MC3T3-E1 cell migration speed on flat PDMS, nanopillars, silicon oxide, and titanium oxide. (b) Changes in aspect ratio over 16 h. (c) Cell elongation on different surfaces. One-way ANOVA and Tukey's post hoc test, NS – not significant, ***p <0.001.

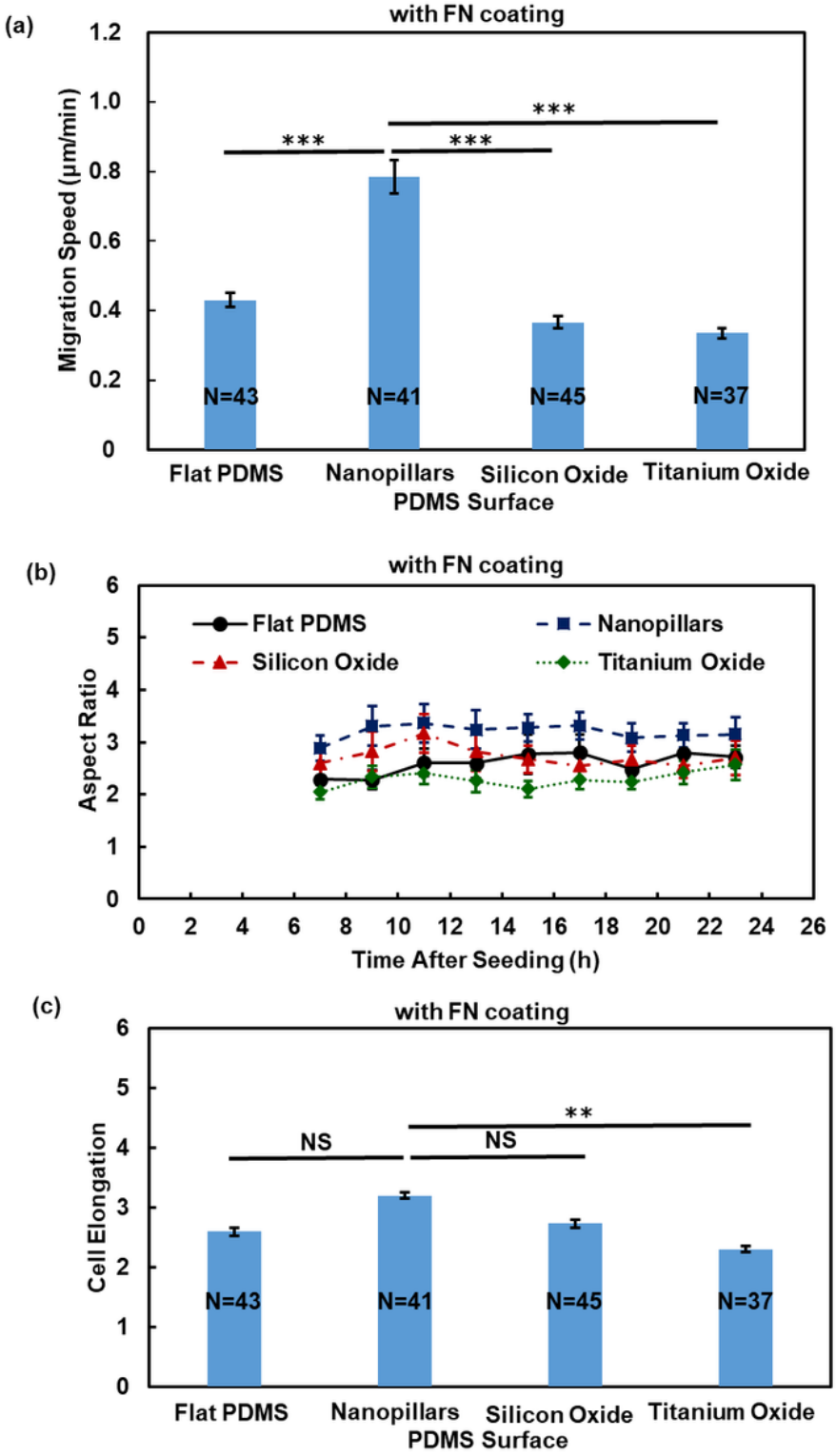

Figure 4

All surfaces were coated with FN. (a) MC3T3-E1 cell migration speed on flat PDMS, nanopillars, silicon oxide, and titanium oxide. (b) Changes in aspect ratio over 16 h. (c) Cell elongation on different surfaces. One-way ANOVA and Tukey's post hoc test, NS – not significant, **p <0.01, and ***p <0.001.

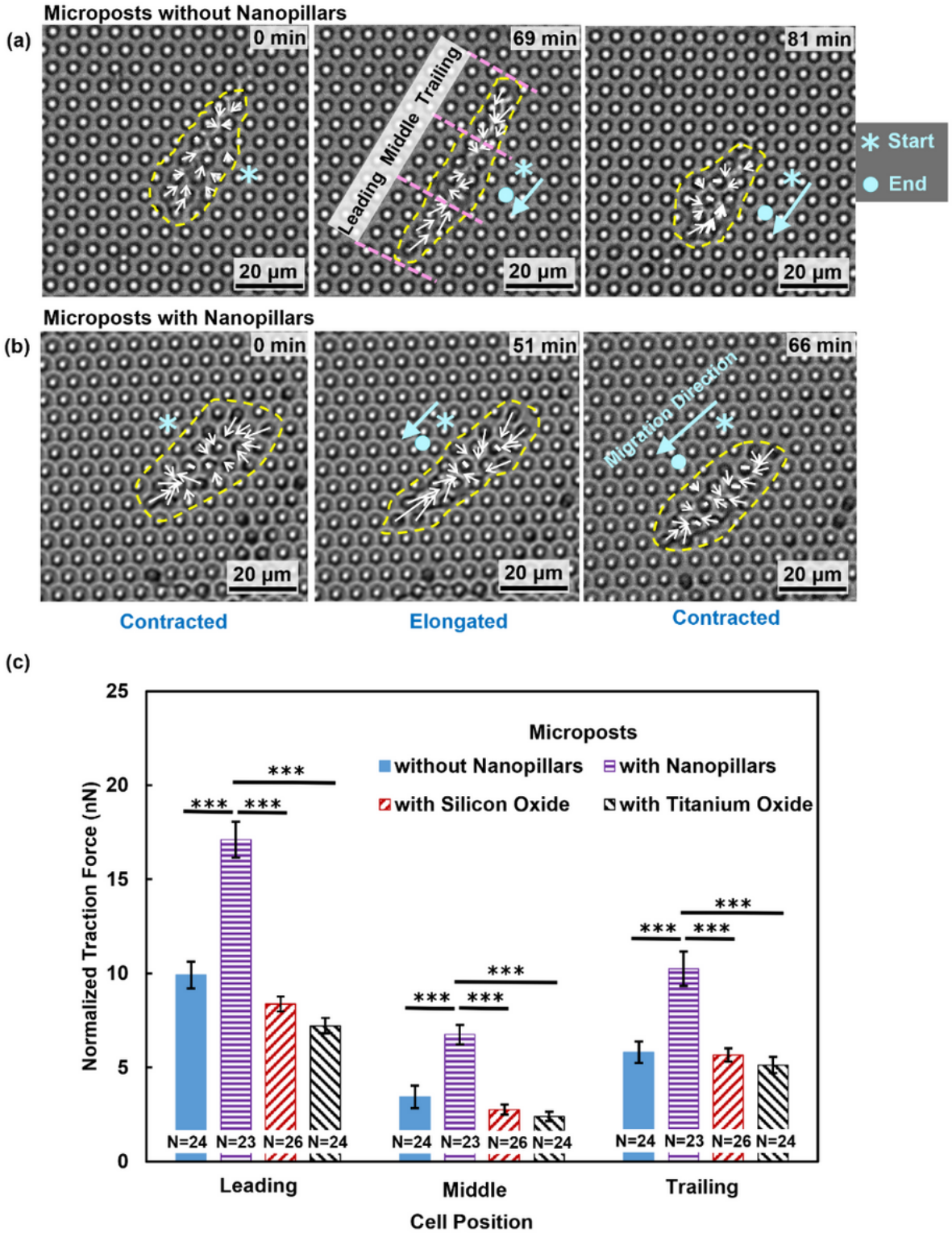

Figure 5

Traction force development for MC3T3-E1 cell migration on PDMS microposts (a) without and (b) with nanopillars. (c) Normalized traction force in leading, middle, and trailing regions of cells on microposts with various surface conditions. Microposts were coated with FN on top and Pluronic on sidewalls. The yellow dashed line indicates cell contour. The starting and ending positions are indicated by asterisks and dots in the micrographs, respectively. The white arrows indicate the traction force on microposts. The

length of the white arrow represents the magnitude of the traction force. Cell migration direction is marked by a blue arrow, representing the movement of the cell centroid during a single migration cycle. One-way ANOVA and Tukey's post hoc test, ***p <0.001.

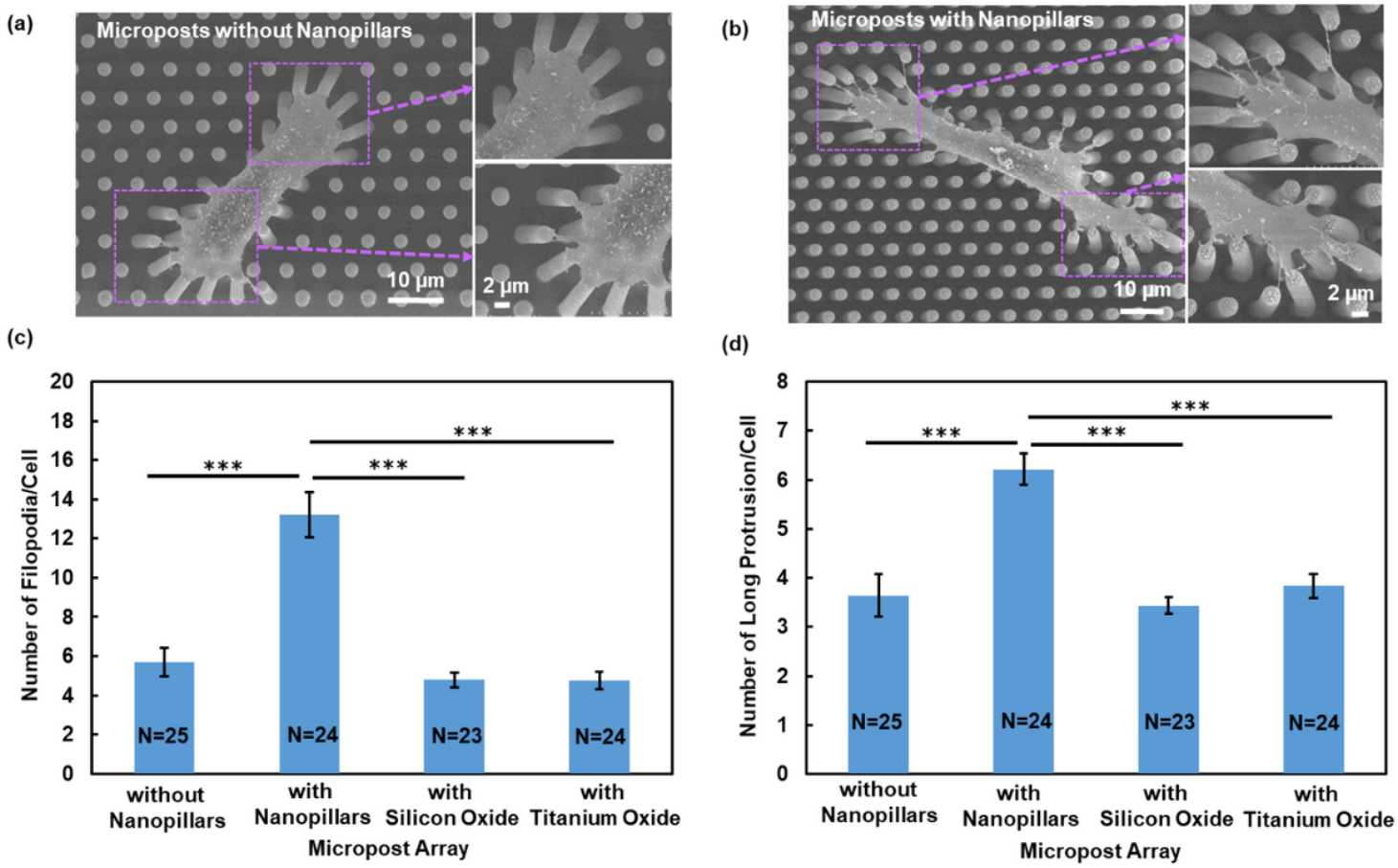

Figure 6

Micrographs of MC3T3-E1 cells on microposts (a) without nanopillars and (b) with nanopillars. Number of (c) filopodia and (d) long protrusions per cell from scanning electron micrographs. Microposts were coated with FN on top and Pluronic on sidewalls. One-way ANOVA and Tukey's post hoc test, ***p <0.001.

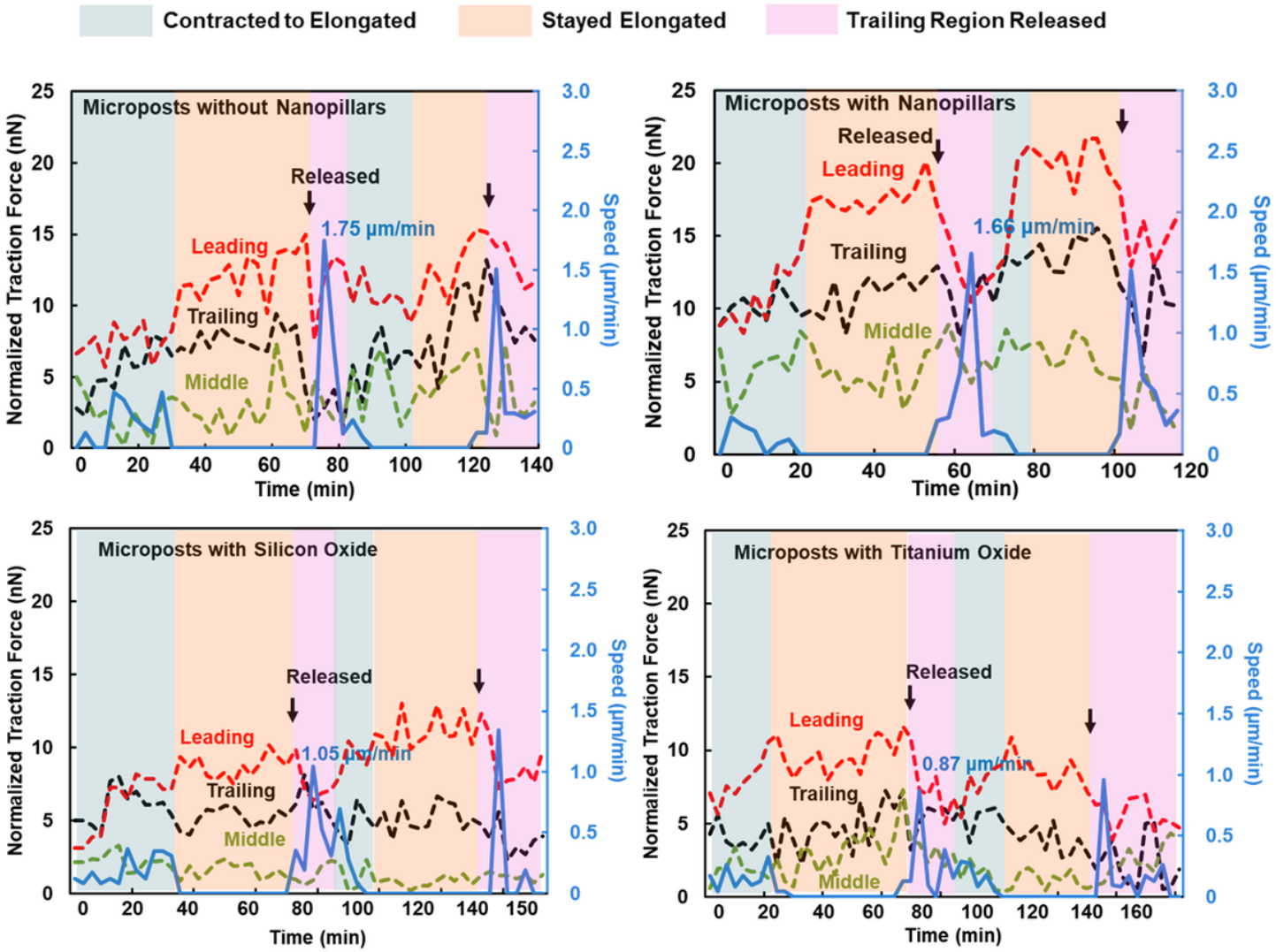

Figure 7

Normalized cell traction force and speed as function of time for MC3T3-E1 cells migrated on PDMS microposts (a) without nanopillars, (b) with nanopillars, (c) with silicon oxide, and (d) with titanium oxide. Microposts were coated with FN on top and Pluronic on sidewalls. The maximum instantaneous speed is indicated.

Supplementary Files

This is a list of supplementary files associated with this preprint. Click to download.

- SupplementaryFiguresSubmit.pdf
- SupplementaryMovieSubmit.mp4